Electronic Supplementary Material (ESI) for Nanoscale.

Supporting Information

Oxidation-stable plasmonic copper nanoparticles in photocatalytic TiO_2 nanoarchitectures

Paul A. DeSario,* Jeremy J. Pietron,* Todd H. Brintlinger,[♠] Monica McEntee,[♦] Joseph F. Parker, Olga Baturina, Rhonda M. Stroud,[♠] Debra R. Rolison

Chemistry Division (Code 6100) and [♠]Materials Science and Technology Division (Code 6300),
U. S. Naval Research Laboratory, Washington, D. C. 20375, USA

[♦]U.S. Edgewood Chemical Biological Center, 5183 Blackhawk Rd., Aberdeen Proving Ground,
MD 21010

Calculated localized surface plasmon resonance extinction

Static spectra of localized surface plasmon resonance (LSPR) bands for Cu nanoparticles were calculated using standard Mie-theory expression for the extinction coefficient of spherical nanoparticles [1]

$$\sigma_{ext} = \frac{9V \in_m{}^{3/2}}{c} \frac{\omega \epsilon_2}{[\epsilon_1 + 2\epsilon_m]^2 + \epsilon_2{}^2}$$

where V is the particle volume, ω is the frequency of light, $\in_m$ is the dielectric constant of the medium, and ϵ_1 and ϵ_2 are the real and imagninary components of the complex dielectric function, respectively. The optical constants used are those reported by Rakic et al.[2] Extinction of 5-nm diameter spherical Cu nanoparticles was calculated as a function of refractive index from n=1.6–2.66 (Fig. S1a) covering a broad range with varying degrees of contributions from air (n=1), TiO_2 (n=2.5), Cu_2O (n=2.4), and CuO (n=2.66).

Static spectra of LSPR bands of prolate Cu ellipsoids were calculated as a function of aspect ratio using the standard Gans-theory expression for the extinction coefficient of ellipsoids[3]

$$\sigma_{ext} = \frac{2\pi NV \in_m{}^{3/2}}{3\lambda} \sum_j \frac{\left(1/P_j{}^2\right)\epsilon_2}{\left(\epsilon_1 + \frac{1-P_j}{P_j}\epsilon_m\right)^2 + \epsilon_2{}^2}$$

where N is the number density of particles, λ is the wavelength of light, and P_j is the depolarization factor for each axis (A, B, and C) of the ellipsoid (Fig. S2a). For prolate ellipsoids, A and B are the long and short axes and A>B=C; the aspect ratio is the ratio of the long axis (A) to the short axis (B). Extinction was calculated for aspect ratios ranging from 1–3. The ellipcity (e) and depolarization constants are given by

$$e = \sqrt{1 - \left(\frac{B}{A}\right)^2}$$

$$P_A = \frac{1 - e^2}{e^2}\left[\frac{1}{2e}\ln\left(\frac{1 + e}{1 - e}\right) - 1\right]$$

$$P_B = P_C = \frac{1 - P_A}{2}$$

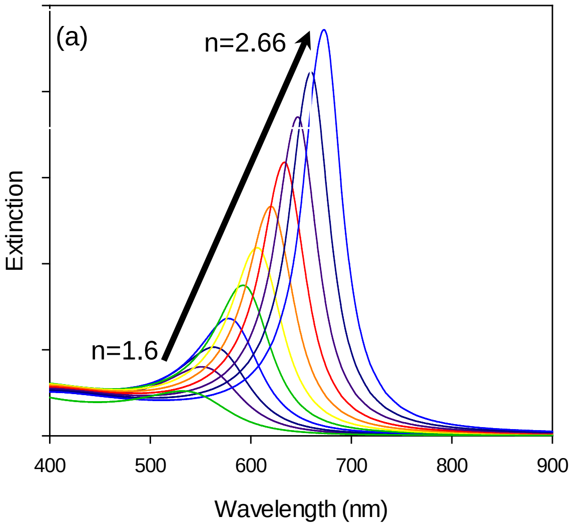

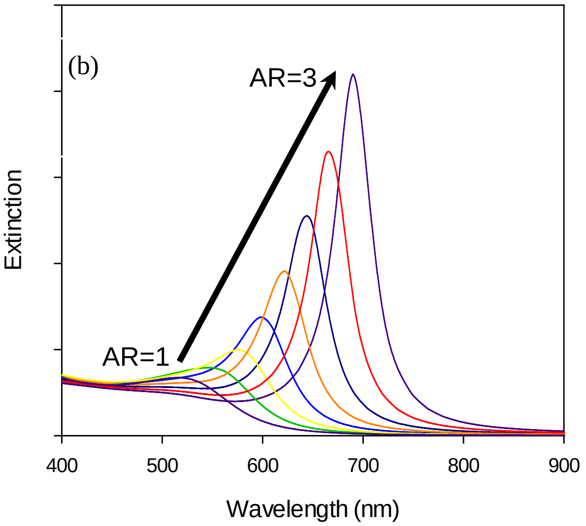

Fig. S1. (a) Mie theory calculations of SPR bands of 5-nm diameter spherical Cu nanoparticles as a function of refractive index ranging from n=1.6–2.66 covering the range that comprises a mixture of air (n=1) and some combination of oxides including TiO_2 (n=2.5), Cu_2O (n=2.4), and CuO (n=2.66); (b) Gans-Theory calculations of SPR bands of prolate ellipsoidal particles as a function of aspect ratio; refractive index of the medium held constant at n=1.42.

Electron Microscopy

Using aberration-corrected scanning transmission electron microscopy (STEM), the plane spacing of Cu nanparticles in Cu/TiO_2[aerogel/24] were measured using high-magnification high-angle annular dark field (HAADF) imaging (Fig. S2). Candidate Cu particles were first identified according to HAADF intensity contrast, and then lattice spacing was measured with a line profile for those particles with lattice planes parallel to the beam. The plane spacing of 0.208 nm matching Cu(111) was measured for the region identified in Fig. S2a by averaging over ten full periods (Fig. S2b). The reciprocal space measurement was used to calibrate the image relative to the more abundant plane spacing of anatase TiO_2, whose presence was easily verified by XRD. With the anatase spacing acting as self-calibration, a relative uncertainty of 1% in spatial calibration allows for disambiguation between metallic Cu(111) at 0.208 nm and the 0.213 nm spacing of Cu_2O(200).

To complement (S)TEM data in Fig. 4 and Fig. 5 of the main text, using the same tools and procedures as outlined previously, additional electron microscopy was performed on both a copper-modified aerogel with a 6-h exposure to argon (Cu/TiO_2[aerogel/6], Figs. S3, S4) as well as a free-standing Cu particle on a lacey carbon TEM grid (Fig. S5). The particle size and shape distribution for Cu/TiO_2[aerogel/6] (Fig. S3) looks the same as that relative to Cu/TiO_2[aerogel/24] (main text, Fig. 4) in the low magnification in image (a) and also the distinct lattice lines for metallic copper in HRTEM are apparent for both (b). A metallic Cu particle identified by inverse-FFT image made by masking the Cu(111) reflection is identified in panel (b). The background-subtracted EELS spectrum in (c) also shows the metallic-type line shape in addition to a weak bright/white/sharp edge indicative of oxidized copper, indicating the presence of some Cu oxide in addition to Cu(0). Metallic Cu regions are also evidenced by collecting site-specific energy-dispersive X-ray spectroscopy (EDS) in regions where potential Cu nanoparticles were identified.

The EDS mapping recorded concurrently with (S)TEM HAADF imaging reveals minimal oxygen co-located with Cu regions. In S5, we contrast with an isolated Cu particle free of the TiO_2 support. The lattice spacing of CuO or tenorite (Fig. S5a) is easily identified for the freestanding particle and the background-subtracted EELS spectrum from this particle (Fig. S5b) has the bright/white/sharp peak feature associated with oxidized copper.

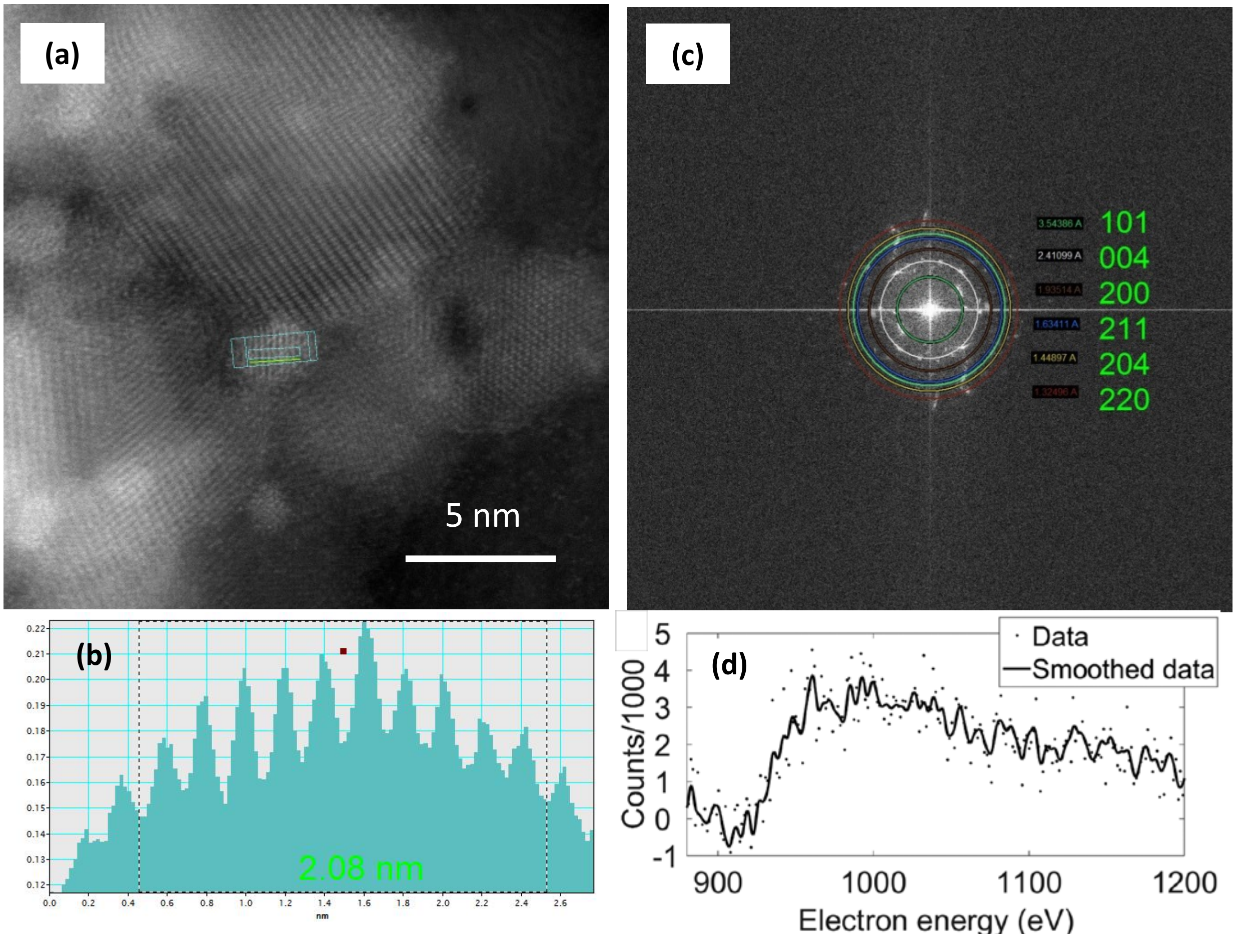

Fig. S2. (a) HAADF TEM of 24-h reduced copper at TiO_2 showing profile box where lattice spacing was measured; (b) (b) a HAADF profile spanning 10 periods; (c) The FFT showing anatase lattice spacings with Cu also present but much weaker; (d) Electron energy-loss spectroscopy (EELS) of the Cu particle identified in (a) collected with 0.5 eV dispersion.

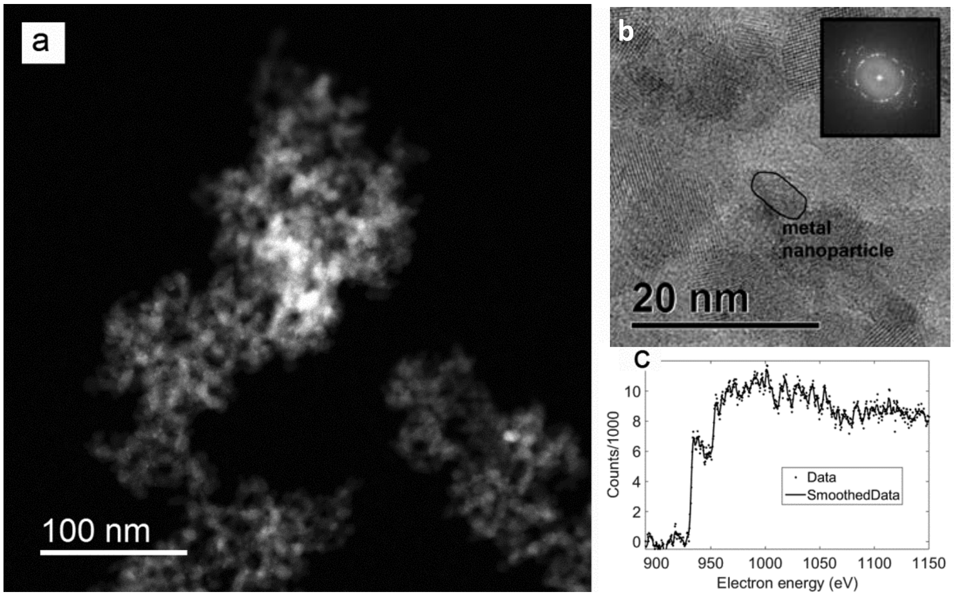

Fig. S3. (a) STEM-HAADF of Cu/TiO_2[aerogel/6]; (b) High-resolution transmission electron micrograph and a metallic Cu nanoparticle (outlined) showing lattice spacing matching Cu(111); (c) Electron energy–loss spectroscopy of Cu/TiO_2 aerogel[6] taken from different sample. The Cu nanoparticle outlined in (b) was initially identified by performing an inverse FFT while masking the Cu(111) region of the FFT.

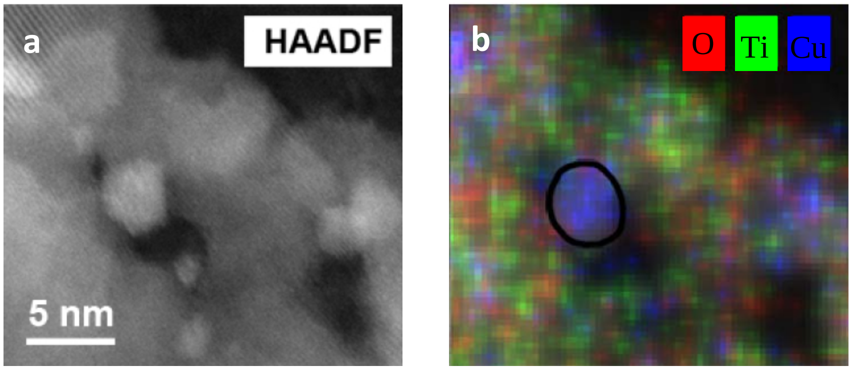

Fig. S4. (a) The STEM-HAADF of Cu/TiO_2[aerogel/6] and (b) site-specific energy-dispersive spectra (EDS) composite map collected simultaneously with STEM-HAADF images show minimal oxygen co-located with the copper, suggesting predominantly metallic nanoparticles.

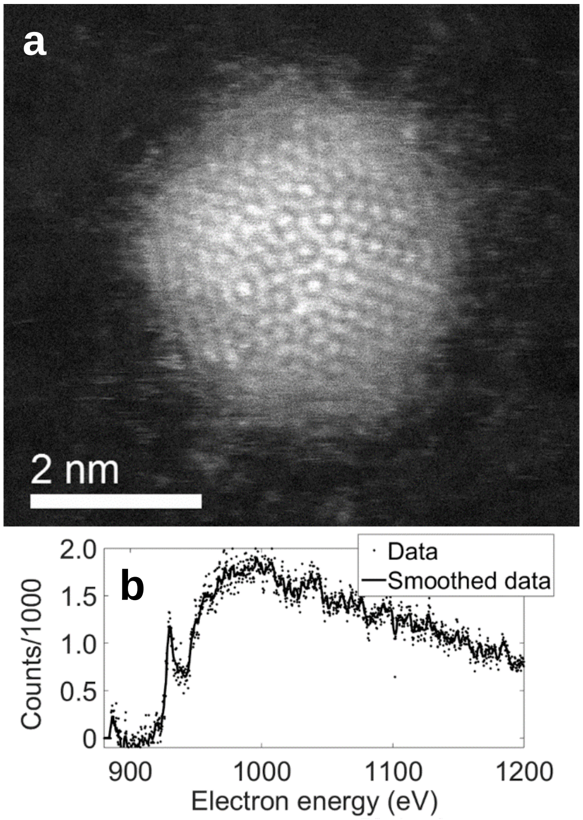

Fig. S5. (a) The STEM-HAADF of bare Cu particle on lacey carbon with CuO lattice; (b) Electron-energy loss spectroscopy showing sharp/bright/white edge indicative of oxidized copper.

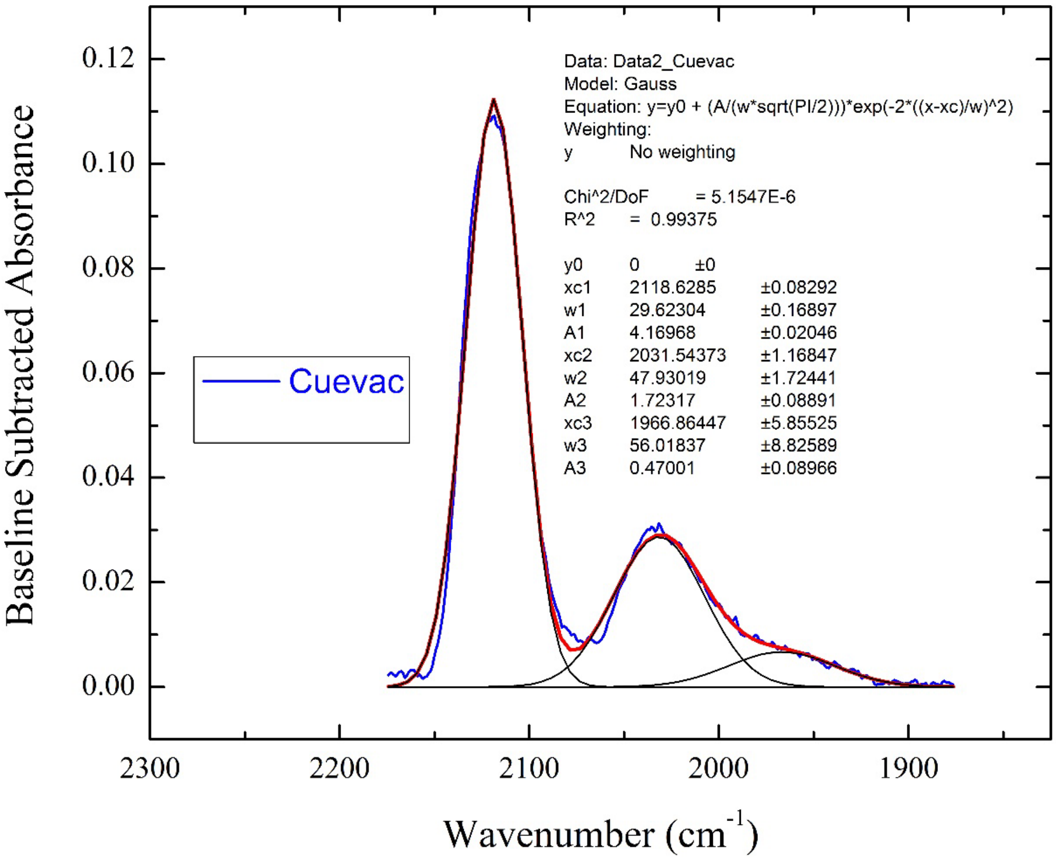

```
Data: Data2_Cuevac
Model: Gauss
Equation: y=y0 + (A/(w*sqrt(PI/2)))*exp(-2*((x-xc)/w)^2)
Weighting:
y          No weighting

Chi^2/DoF        = 5.1547E-6
R^2       =  0.99375

y0        0           ±0
xc1       2118.6285         ±0.08292
w1        29.62304          ±0.16897
A1        4.16968           ±0.02046
xc2       2031.54373        ±1.16847
w2        47.93019          ±1.72441
A2        1.72317           ±0.08891
xc3       1966.86447        ±5.85525
w3        56.01837          ±8.82589
A3        0.47001           ±0.08966
```

Fig. S6. Transmission IR spectrum of Cu/TiO_2[aerogel/24] after dosing with 2.4 Torr CO(g) and subsequent evacuation including Guassian peak fitting for Cu(0) mode at ~2034 cm^{-1} and Cu(I) mode at 2118 cm^{-1}.

Table S1. Examples of plasmonic properties of nanostructured Cu.

Reference*	Materials	Optical properties	Comments
7	10 nm dia. Cu on 100 nm dia. TiO_2 nanotube arrays	SPR at ~550 nm	•No protective layers utilized; •Active for visible light driven H_2 evolution in 5% ethylene glycol
8	20-40 nm Cu photodeposited on commercial TiO_2; Cu coated with poly vinyl alcohol (PVA)	•SPR at 600 nm •Red shifts to 625nm when coated with PVA	SPR extinction disappeared when exposed to air unless Cu particles protected with PVC
17	15 nm dia. Cu nanoparticles supported on graphene via reduction of Cu_2O with H_2/Ar	SPR at 560 nm	Active for coupling reactions of aromatic nitro compounds to azoxy or azo compounds under visible excitation
18	50 nm diameter Cu nanoplates reduced with hydrazine and coated with polyvinylpyrrolidone (PVP)	SPR at 600 nm when stabilizer is present; dampens and red-shifts when oxidized	Stable for days in air with PVP stabilized but fully oxidized in 1 day in air without PVP stabilizer
19	80 nm dia. x 20 nm tall Cu discs on SiO_2 or TiO_2 via e-beam evaporation	•SPR@ 640 nm on SiO_2 and 740 nm on TiO_2	Cu oxidized on TiO_2 support after illumination with UV light; SPR damped and blue-shifted when oxidized
20	12 nm dia. Cu colloids capped with oleic acid	•SPR@ 600 nm •SPR maxima and stability of Cu particle dependent upon solvent	Colloids oxidized and formed oxide shell when oleic acid cap removed; SPR shifted to 750 nm with oxide shell
21	•Cu nanoparticle arrays deposited via nanosphere lithography •20–70 nm thick Cu layer deposited between nanosphere templates ranging in dia. between 280–590 nm	•SPR maxima at ranging from 670-764 nm •SPR blue shifts for smaller dia. template and increased Cu thickness	Oxide-free in N_2 atmosphere after reduction with acetic adic but oxidized when exposed to ambient air
22	41 nm dia. Cu on SiO_2 support	•SPR max at 590 nm for fully reduced Cu •red-shifts and dampens when exposed to photocatalytic conditions	•Metallic Cu shows higher selectivity for propylene epoxidation •Cu particles oxidize when exposed to photocatalytic conditions and re-reduce in H_2 atmosphere or by SPR excitation
23	3 nm diameter Cu	•SPR@570nm in vaccum •650 nm after oxidation in air	•Heating in air oxidized Cu particles •Forms Cu_2O at lower temperature and CuO at higher temperature
24	Cu supported on glass via chemical deposition of Cu or reduction of Cu_2O with $NaBH_4$	•SPR@650 nm for chemically deposited Cu •SPR@720 nm for chemically reduced Cu	Red shifts with increased diameter and red shifts and dampens when exposed to air
25	Cu nanoparticles via thermal reduction with graphite in phosphate glass	SPR@580 nm	
40	30–100 nm Cu nanoparticles photodeposited on TiO_2 support	SPR@ 590–610 nm, increasing with increased Cu diameter	No protective layers used
41	22 nm dia. Cu@Cu_2O core-shell nanoparticles via RF-sputtering and RF-PECVD	Calculated SPR max ranges from ~570–690 nm depending upon core size and shell thickness	•SPR damped and blue-shifted with decreasing core size •SPR damped with increasing shell thickness
50	50 nm dia. Cu nanoparticles via UV photoreduction of Cu_2O on TiO_2 support	No SPR peak; lack of SPR attributed to agglomeration of Cu particles	Demonstrated photocatalytic water reduction under visible light; photocatalytic activity diminished when catalyst exposed to air

*Refers to reference number from the main text.

REFERENCES

---

1. Link, S.; El-Sayed, M.A. Size and temperature dependence of the plasmon absorption of colloidal gold nanoparticles. *J. Phys. Chem. B* **1999**, *103*, 4212–4217.
2. Rakić, A.D.; Djurišić, A.B.; Elazar, J.M.; Majewski, M.L. Optical properties of metallic films for vertical-cavity optoelectroic devices. *Appl. Optics* **1998**, *37*, 5271–5283.
3. Link, S.; El-Sayed, M.A. Spectral properties and relaxation dynamics of surface plasmon electronic oscillations in gold and silver nanodots and nanorods. *J. Phys. Chem. B* **1999**, *103*, 8410–8426.